arXiv:cond-mat/0510068v1 [cond-mat.soft] 4 Oct 2005

Static and dynamic properties of the interface between a polymer brush and a melt of identical chains

C. Pastorino and K. Binder
Institut für Physik WA331, Johannes Gutenberg-Universität, 55099, Mainz, Germany

T. Kreer
Institut Charles Sadron, 6 Rue Boussingault, 67083 Strasbourg, France

M. Müller
Department of Physics, University of Wisconsin-Madison, WI 53706-1390, USA and
Institut für Theoretische Physik, Friedrich-Hund-Platz 1, 37077 Göttingen, Germany

Molecular dynamics simulations of a short-chain polymer melt between two brush-covered surfaces under shear have been performed. The end-grafted polymers which constitute the brush have the same chemical properties as the free chains in the melt and provide a soft deformable substrate. Polymer chains are described by a coarse-grained bead-spring model with Lennard-Jones interactions between the beads and a FENE potential between nearest neighbors along the backbone of the chains. The grafting density of the brush layer offers a way of controlling the behavior of the surface without altering the molecular interactions. We perform equilibrium and non-equilibrium Molecular Dynamics simulations at constant temperature and volume using the Dissipative Particle Dynamics thermostat. The equilibrium density profiles and the behavior under shear are studied as well as the interdigitation of the melt into the brush, the orientation on different length scales (bond vectors, radius of gyration, and end-to-end vector) of free and grafted chains, and velocity profiles. The viscosity and slippage at the interface are calculated as functions of grafting density and shear velocity.

I. INTRODUCTION

Grafted polymer layers have received abiding attention because coating surfaces with polymer brushes offers an opportunity to control static and dynamic surface properties. Polymer brush coatings have been utilized in a wide variety of applications ranging from the stabilization of colloidal suspensions (e.g., paint), the reversibly tuning of wetting and adhesion properties to lubrication, friction and wear.[1] For instance, polymer brushes are renown for their ability to drastically decrease the friction between two solid surfaces.[2] The work of adhesion and wettability are also changed when a solid surface is coated with end-grafted polymer layers. Thus, polymer brushes and cross-linked rubbers find applications as adhesives.

Polymer brushes are also interesting from a fundamental point of view because many properties are determined by the conformational entropy of the extended macromolecules, in particular, the stretching of the polymers away from the grafting surface[3] in response to increasing the grafting density or swelling the brush with a solvent. Increasing the grafting density is an experimentally convenient way of altering the surface properties without altering molecular interactions. This gives rise to a rich wetting behavior even in apparently simple model systems like a polymer drop on top of a brush of identical chains.[4–8] If there are few chains grafted onto the surface, an increase of the grafting density will result in a smaller contact angle because the melt chains benefit from the additional attraction provided by the brush. At intermediate grafting densities this might result in complete wetting of the melt on the top of brush. If the grafting density is too high, however, the polymer melt will dewet from the brush – a phenomenon termed autophobicity. Such "entropic dewetting" has been observed experimentally in polymer networks[9] and polymer brushes.[10,11] Autophobicity can be traced back to the formation of an interface between the strongly stretched chains in the polymer brush and the free chains of the melt.[4–7]

The interface between brush and melt has many important applications: Such interfaces commonly occur between two immiscible homopolymers that have been reinforced by a diblock copolymer. The diblock adsorbs at the interface as to place its blocks into the respective phases. Thereby, it lowers the interfacial tension and, for sufficiently large surface excess, each block forms a polymer brush in contact with the homopolymer-rich bulk phase.[12,13] The interdigitation between brush and homopolymer chains determines many mechanical properties of the interface.[14,15] While the equilibrium properties of these copolymer brushes at the interface between incompatible homopolymers (as well as brushes formed from end-adsorbed chains) resemble those of irreversibly grafted polymer brushes, their dynamic properties might substantially differ due to the in-plane mobility. Another realization of a brush-melt interface occurs when a polymer melt dewets from a dense polymer brush (or rubber[9]). These soft deformable substrates might offer great control over flow properties. As we shall demonstrate below, changing the grafting properties one can tune the hydrodynamic boundary conditions. If the grafting density is high enough for autophobic dewetting to occur,, additional mechanisms of dissipation for moving droplets like lifting of the three-phase contacts line (wetting ridge)[16] to balance the normal components of the forces on the contact line or chain pull-out[17] can be envisaged.

The equilibrium properties of polymer brushes in various solvents have been studied by Monte Carlo[18,19] and Molecular Dynamics (MD) simulations[20–23] as a function of chain length and grafting density. There are fewer studies investigating the equilibrium properties of the brush-melt interface. Grest studied the limit in which the melt chains are much shorter than the chains of the brush.[21] Daoulas *et al.* performed detailed atomistic Monte Carlo simulations to analyze the equilibrium structure a chemically realistic united atom model for polyethylene melt in contact with a brush grafted onto a carbon substrate.[23] These brush-melt interfaces of long entangled chains have also been investigated in the context of adhesion. Sides and Grest used glassy brush-melt interfaces to study chain pull-out and craze formation under tensile stress by means of simulations.[24]

Although the molecular mechanisms and the concomitant boundary conditions (amount of slip) of flow at polymeric interfaces have attracted abiding interest, it is only incompletely understood. Many distinct physical processes are involved such as wetting, roughness and bubble formation.[25] An accurate prediction of non-equilibrium properties is important for the design of nano- and microfluidic devices characterized by a large surface-to-volume ratio. In particular, the boundary condition of polymer melts between walls has been extensively studied experimentally,[26,27] by computer simulation[28,29] and by analytic theory.[30,31] The boundary condition and friction mechanisms have also been studied experimentally with near field laser velocimetry techniques, including anchored chains in the solid surface.[27] The sliding of two brushes and the non-equilibrium behavior of brush-brush interfaces can be studied by surface force apparatus (SFA) measurements[2] and the experimental results have been compared with computer simulations.[21,22,32,33] These simulations emphasize the correlation between the non-equilibrium shear properties and the interdigitation and orientation of the two apposed brushes.

In this work we study the behavior of the brush-melt interface of short non-entangled chains of a coarse-grained model in equilibrium and under shear as a function of the two experimentally accessible parameters: grafting density and shear velocity. The grafting density is systematically varied over a wide range from the mushroom-regime to high grafting densities that correspond to autophobic behavior. MD simulations in junction with the Dissipative Particle Dynamics thermostat are employed to account for hydrodynamic correlations without including an explicit solvent. Unlike most calculations in the literature we study polymer chains in a poor solvent. The attraction between monomers allows us to extend this model to studying liquid-vapor interfaces and the wetting of a melt on top of a brush of identical chains. The remainder of our manuscript is organized as follows: In section II we introduce our coarse-grained model and the simulation technique. In section III the results of the simulations for the structure, orientations and boundary conditions of this melt-brush interface in equilibrium and under shear are detailed. The last sections contains a discussion of our results and an outlook on future work.

II. MODEL AND THERMOSTAT

We consider a widely utilized, coarse-grained bead-spring model for polymers.[34] This model has been used for a variety of thermodynamic conditions, chain lengths and physical regimes such as glasses, melts and dilute solutions.[35] The potential between neighboring beads along the same polymer is modeled by a finite extensible non-linear elastic potential (FENE) ,

$$U_{\text{FENE}} = \begin{cases} -\frac{1}{2}k\ R_0^2 \ln\left[1-(\frac{r}{R_0})^2\right] & r < R_0 \\ \infty & r \geq R_0 \end{cases}, \quad (1)$$

where $R_0 = 1.5\sigma$, the spring constant is $k = 30\epsilon/\sigma^2$, and $r = |\mathbf{r}_i - \mathbf{r}_j|$ denotes the distance between neighboring monomers. Excluded volume interactions at short distances and van-der-Waals attractions between segments are described by a truncated and shifted Lennard-Jones (LJ) potential:

$$U(r) = U_{\text{LJ}}(r) - U_{\text{LJ}}(r_c)\,, \quad (2)$$

with

$$U_{\text{LJ}}(r) = 4\epsilon\left[\left(\frac{\sigma}{r}\right)^{12} - \left(\frac{\sigma}{r}\right)^{6}\right] \quad (3)$$

where the LJ parameters, $\epsilon = 1$ and $\sigma = 1$, define the units of energy and length, respectively. $U_{\text{LJ}}(r_c)$ is the LJ potential evaluated at the cut-off radius of twice the minimum of the potential: $r_c = 2 \times 2^{\frac{1}{6}}$. Often a completely repulsive LJ potential, $r_c = 2^{\frac{1}{6}}$, has been utilized for computational efficiency.[32,33,36] This choice corresponds to a polymer brush in a good solvent. Here, we include attractive interactions between segments and, thus, are able to describe liquid-vapor coexistence, wetting and droplet formation below the Θ-temperature, $k_B\Theta/\epsilon \sim 3.3$.[37]

The substrates at $z = 0$ and $z = D$ are modeled as idealized flat and impenetrable walls which interact with the polymer segments via an integrated Lennard-Jones potential, of the form

$$V_{\text{wall}}(z) = |A|\left(\frac{\sigma}{z}\right)^{9} - A\left(\frac{\sigma}{z}\right)^{3},$$

where $A = 3.2\epsilon$ is sufficient to make the liquid wet the bare substrate.[37]

The lateral positions of the grafted chain heads are randomly chosen with a total number of chains given by the desired grafting density. The distance of the first bead from the grafting surface is $z_1 = 1.2\sigma$.

In our model wall roughness is completely disregarded. The friction between the melt of free chains and the surface stems from the grafted chains only. Our goal is to analyze the experimentally controllable properties of the substrate provided by the grafted polymer layer without any additional source of roughness arising from a possible corrugation of the substrate.

We used a Dissipative Particle Dynamics thermostat (DPD) to simulate at constant temperature[38,39] and account for hydrodynamic interactions due to the conservation of total momentum. The equations of motion are formally the same as used in Langevin dynamics:[40,41]

$$\dot{\mathbf{r}}_i = \frac{\mathbf{p}_i}{m_i} \qquad (4)$$

$$\dot{\mathbf{p}}_i = \mathbf{F}_i + {\mathbf{F}_i}^D + {\mathbf{F}_i}^R \qquad (5)$$

where ${\mathbf{F}_i}^D$ and ${\mathbf{F}_i}^R$ denote the dissipative and random forces respectively. m_i is the mass of the monomers which is set to unity for all the simulations. The difference between DPD and Langevin thermostats is that the random and dissipative forces are applied in a pair-wise form, where the total forces acting on a pair are equal to zero and, thus, momentum conservation is obeyed. The expression for the forces are the following:

$${\mathbf{F}_i}^D = \sum_{j(\neq i)} \mathbf{F}^D_{ij} \quad ; \quad \mathbf{F}^D_{ij} = -\gamma\omega^D(r_{ij})(\hat{\mathbf{r}}_{ij}\cdot\mathbf{v}_{ij})\hat{\mathbf{r}}_{ij} \qquad (6)$$

$${\mathbf{F}_i}^R = \sum_{j(\neq i)} \mathbf{F}^R_{ij} \quad ; \quad \mathbf{F}^R_{ij} = \zeta\omega^R(r_{ij})\theta_{ij}\hat{\mathbf{r}}_{ij}, \qquad (7)$$

where for each vector $\mathbf{a}$ we use a notation $\mathbf{a}_{ij} = \mathbf{a}_i - \mathbf{a}_j$, γ is the friction constant and ζ denotes the noise strength. Friction and noise, γ and ζ, obey the relation $\zeta^2 = 2k_BT\gamma$ and the concomitant weight functions satisfy fluctuation-dissipation theorem, $[\omega^R]^2 = \omega^D$. θ_{ij} is a random variable with zero mean and second moment $\langle\theta_{ij}(t)\theta_{kl}(t^{'})\rangle = (\delta_{ij}\delta_{jl} + \delta_{il}\delta_{jk})\delta(t-t^{'})$ and the weight functions are chosen to be:

$$[\omega^R]^2 = \omega^D = \begin{cases}(1-r/r_c)^2, r < r_c & , \\ 0, \quad r \geq r_c\end{cases} \qquad (8)$$

which is a common choice for continuous forces.[42]

The equations of motion (5) were integrated using the velocity Verlet algorithm[40,41] with a time step of $dt = 0.0005\tau$ or $dt = 0.002\tau$ where $\tau = \sigma\sqrt{m/\epsilon}$ denotes the time unit in Lennard Jones parameters. Using the described simulation scheme nVT, non-equilibrium (applied constant shear velocity in the walls) and equilibrium simulations were performed.

We studied a melt of 10-bead polymer chains with segment number density close to $\rho_{\mathrm{melt,coex}}\sigma^3 = 0.61$ between two end-grafted polymer layers of different grafting densities. A temperature of $k_BT/\epsilon = 1.68$ was used to reproduce the thermodynamic conditions of previous Monte Carlo and self-consistent field calculations.[7,37] At this temperature the density, $\rho_{\mathrm{melt,coex}}$, of the melt in coexistence with its vapor of very low density is not too high and an efficient equilibration of the system by Monte Carlo or MD simulations is possible. If we reduced the temperature further the density of the vapor would decrease further but the density of the coexisting melt would increase and, thus, significantly slow down the simulations.

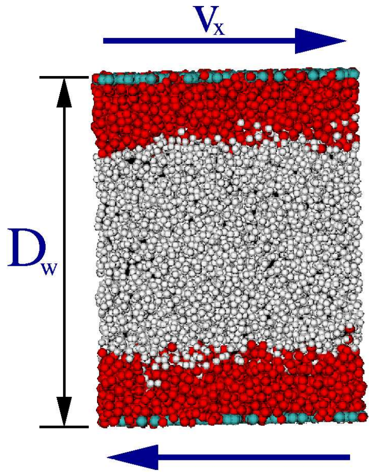

Figure 1: Sketch of the simulation setup. Segments of the free melt chains are shown in light grey, the brush is presented in dark grey, while the heads of the brush are light. The figure corresponds to a snapshot of the simulation box for a grafting density of $R^2_{ee}/\Sigma = 5.89$ and wall velocity $v_x = 1\sigma/\tau$ The shear direction, wall velocity and distance between walls are indicated.

The grafting density Σ^{-1} denotes the number of grafted chains per unit area and we measure it in units of the end-to-end distance, R_{ee} of melt chains in the bulk. $R^2_{ee}/\Sigma \sim \mathcal{O}(1)$ marks the cross-over from mushroom to brush regime. The system was simulated for $R^2_{ee}/\Sigma =$ 0.80, 1.47, 2.95, 5.89, 10.31, spanning different physical regimes of the grafted layer – from the mushroom regime for low grafting densities to dense, strongly stretched brushes exhibiting autophobic wetting behavior. Two smaller grafting density values, $R^2_{ee}/\Sigma = 0.27, 0.54$, were also considered to analyze the effective boundary condition of the melt under shear. The area of the grafting substrate was taken to be $21\sigma\times18.2\sigma$, whereas we chose a fixed distance of $D_w = 30\sigma$ between the substrates. The system was simulated typically for 1×10^6 MD steps for thermalization, while trajectories of length 2.6 to 4×10^6 were used to average data subsequently. The walls were sheared relative to each other in the lateral direction, as shown in Fig. 1, where the main parameters of the simulation are indicated.

The shear velocity was taken in the range $v_{\mathrm{x}} = 0{-}2\sigma/\tau$ (or alternatively shear rates $0 \leq \dot{\gamma}\tau \leq 0.06$). The equilibrium characteristics of the system were obtained from bulk MD simulations with periodic boundary conditions in all the spatial dimensions. From them, we extracted the end-to-end distance, $R_{ee} \equiv \sqrt{\langle R_{ee}^2 \rangle} = 3.66\sigma$, and self-diffusion coefficient, $D = 0.05\sigma^2/\tau$. The characteristic relaxation time of chain conformations is thus given by $\tau^* \equiv R_{ee}^2/D = 268\tau$.

To simulate shear we utilized the same thermodynamic conditions as in the equilibrium simulations but moved the first beads of the grafted chains with constant velocity, v_x, in the $\hat{x}$-direction and monitored the force, F_x, on the grafting points (see Fig. 1). Using the natural time and length scales, τ^* and R_{ee}, we define a characteristic velocity, $v^* = D/R_{ee} = 0.014\sigma/\tau$. The ratio between the shear velocity, v_x, measured in units of v^* and the film thickness, D_w, measured in units of R_{ee} defines the Weissenberg number, $\mathrm{We} = (v_x/v^*)(R_{ee}/D_w) = \dot{\gamma}\tau^*$ which measures the shear rate in units of the relaxation time of the chains. Our simulations span a wide range of Weissenberg numbers for this polymer system: $0 \leq \mathrm{We} \leq 16$. Adimensional units are used in the remaining sections unless explicitly mentioned. Lengths are expressed in units of the chains' end-to-end distance, R_{ee}, in the melt and velocities in terms of the Weissenberg number, We.

III. RESULTS

A. Segment density profiles

First, we illustrate the general structure of the brush-melt interface in equilibrium and under shear by plotting profiles of the number density of segments belonging to grafted and free chains in Fig. 2. The grafting density decreases from top to bottom: R_{ee}^2/Σ = 10.31, 5.89, 2.95, 1.47, 0.80. These values cover the entire regime from strongly stretched brushes to mushroom-like configurations. Upon increasing the grafting density we observe the building-up of an interface between the brush and the melt. For low grafting densities, corresponding to the mushroom regime of the brush, the melt chains reach the substrate. For intermediate grafting densities the brush layer starts to expel the melt chains and their density at the substrate becomes vanishingly small for $R_{ee}^2/\Sigma \geq 2.95$. As we increase the grafting density further, the average density inside the brush exceeds the liquid density, ρ_{melt}, and oscillations in the density indicate fluid-like layering effects inside the brush. The layering becomes more pronounced when one increases the brush density and it is somewhat stronger than in previous simulations[32,33] because the grafting density is higher in our case.

The brush chains stretch and the well-developed interface between melt and grafted chains moves farther away from the grafting surface and becomes narrower. For the highest grafting density studied, $R_{ee}^2/\Sigma = 10.31$, there is only very little interdigitation between brush and melt. It is this interdigitation between brush and melt which is important for the static and dynamic properties of the system.

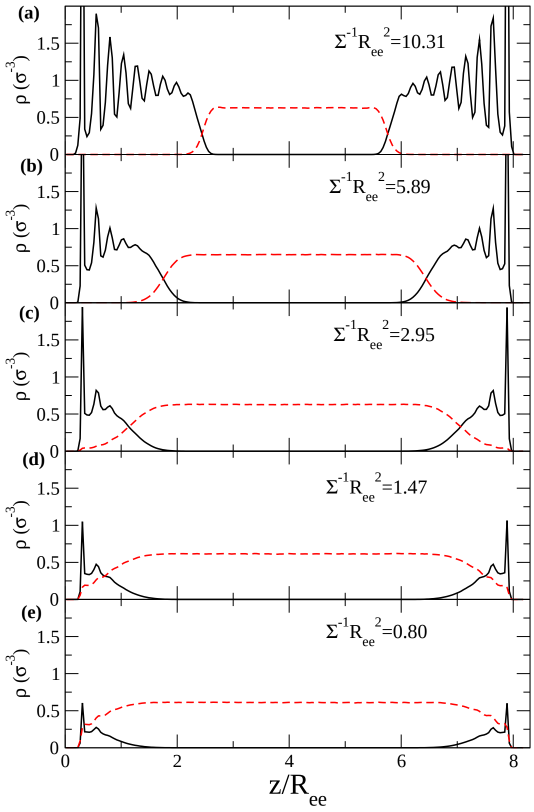

Figure 2: Equilibrium density profiles for various grafting densities. From (a) to (e) the grafting densities decrease: R_{ee}^2/Σ = 10.31, 5.89, 2.95, 1.47, 0.80. Full lines indicate the density of segments belonging to grafted chains while the segment density of free (melt) chains is marked by dashed lines. For all simulations, the melt density is close to the liquid-vapor coexistence density, $\rho_{\mathrm{melt,coex}}\sigma^3 = 0.61$ of the melt at the temperature $k_BT/\epsilon = 1.68$.

To characterize the change of the brush-melt interface as a function of grafting density and shear velocity, we compute the overlap between grafted and free chains:[32]

$$I_{\mathrm{overlap}} = \frac{R_{ee}^2}{N\rho_{\mathrm{melt,coex}}} \int_0^{D_w} \rho_{\mathrm{brush}}(z) \times \rho_{\mathrm{melt}}(z) dz \,, \quad (9)$$

where ρ_{brush} and ρ_{melt} are the brush and melt densities, respectively. The integrand in Eq. (9) is non-zero only in the regions of the film where there are free and grafted polymers and the integral quantifies the total amount of interdigitation. I_{overlap} is directly proportional to the number of interactions between two polymer layers and therefore provides an insight on how the shear stress depends on normal pressure and shear rate.[32,33]

Fig. 3(a) presents the overlap between brush and melt as a function of the grafting density. As we increase the grafting density, the overlap between melt and brush increases because there are more grafted chains at the surface. Upon increasing the grafting density further, however, we observe that the overlap between melt and brush

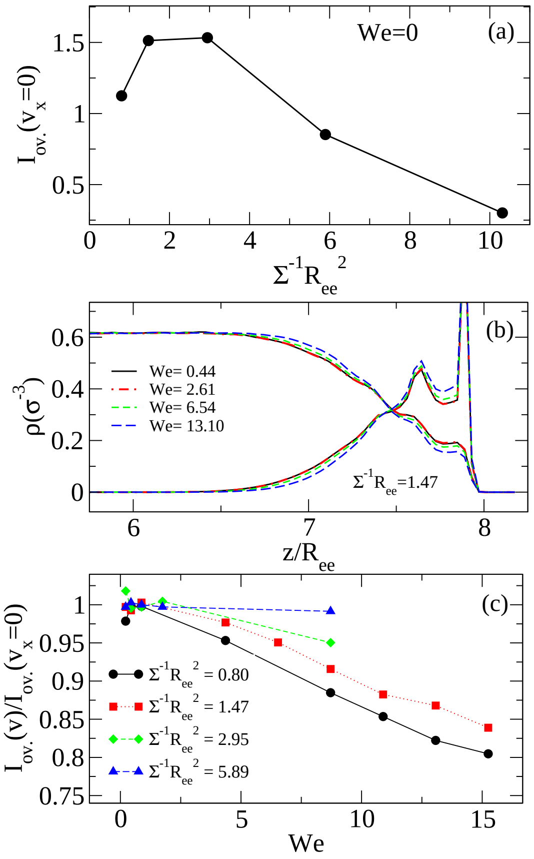

Figure 3: Overlap integral as a function of the grafting density (a). Panel (b) presents the response to shear of the density profiles at intermediate grafting densities. The overlap integral as a funstion of velocity is presented in (c).

passes through a maximum and decreases. The behavior of the overlap between brush and melt parallels the wetting behavior, where one observes that the brush favors wetting of the melt at low grafting densities but leads to autophobic dewetting at large grafting densities.

Panel (b) shows the response of the density profiles to shear for an intermediate grafting density. In qualitative agreement with simulations of polymer brushes in a good continuum or monomeric solvent (cf. Ref. [22] and references therein) the height of the brush decreases upon shear. Here, we observe the behavior for a brush under bad solvent condition immersed into a polymer melt. The thinning of the brush goes along with a significant decrease of the melt-brush interdigitation (cf. panel (c) of Fig. 3), i.e., a sharpening of the brush-melt interface, and it also correlates with the inclination of the grafted polymers for low grafting densities (see subsection III B). For the highest grafting density, $R_{ee}^2/\Sigma = 5.89$, however, the density profiles are almost independent of shear velocity. The chains are so stretched that the shear has less impact on their conformations.

B. Orientation and structure

Next we study conformational and orientation properties. Three distinct phenomena determine the molecular orientation: The grafting substrate or the brush melt interface tend to align the extended molecules parallel to the substrate or interface, respectively. The crowding of the grafted chains at high grafting density results in chain stretching and a perpendicular orientation. Finally, shear tends to align molecules in the direction of the flow.

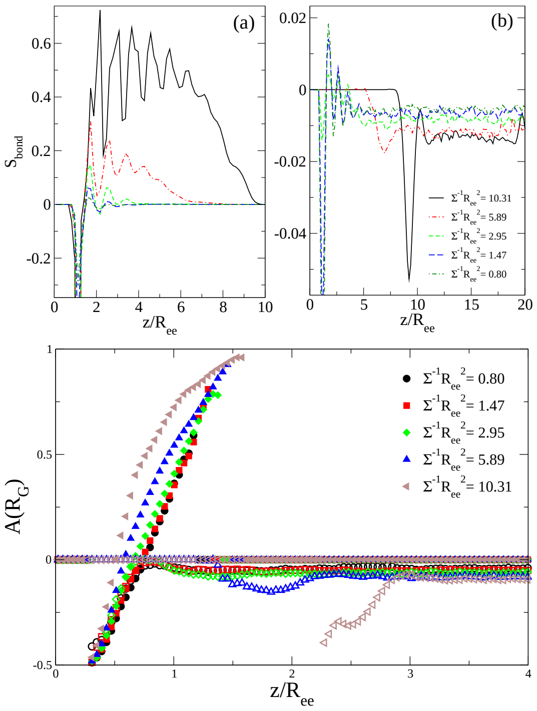

Figure 4: Orientations of the brush-melt interface on different length scales, grafting densities and at fixed shear velocity, $v_x = 1\sigma/\tau$ (or We=8.71). Panels (a) and (b) present the bond orientation of the brush and the melt of free chains, respectively. Part (c) shows the asphericity parameter $A(R_G)$ of the radius of gyration. Full symbol correspond to the chains in the brush while open symbols characterize the behavior of melt chains.

In Fig. 4 the orientation of the grafted layer and melt are shown as a function of the distance, z, from the substrate for various grafting densities. The bond orientation parameter is defined as

$$S_{\text{bond}} = \frac{3\langle\cos^2\theta\rangle - 1}{2}, \tag{10}$$

where θ denotes the angle between the vector connecting two bonded segments and the $\hat{z}$ direction. So defined, $S_{\text{bond}} \sim 1$ characterizes bonds that mainly orient along the $\hat{z}$ direction and $S_{\text{bond}} \sim 0$ corresponds to randomly oriented bonds. $S_{\text{bond}} \sim -0.5$ denotes bonds with an average orientation perpendicular to the substrate (i.e., along the shear direction, $\hat{x}$, if we apply shear). The orientation on the scale of the entire molecule is described by the asphericity order parameter. We define it for the radius of gyration, $\mathbf{R}_G$, and end-to-end vector, $\mathbf{R}_{ee}$, as

$$A(\mathbf{R}) = \frac{R_z^2 - \frac{1}{2}(R_x^2 + R_y^2)}{R_x^2 + R_y^2 + R_z^2}, \tag{11}$$

where R_i (i=x,y,z) denote the different Cartesian components of the considered vector.

$S_{\rm bond}$ for different grafting densities and for Weissenberg number We= 8.71 is presented in Fig. 4. Panel (a) presents the behavior of the grafted chains. In the ultimate vicinity of the grafting surface bonds align parallel similar to the behavior of a melt in contact with a hard substrate. The behavior very close to the grafting surface is largely independent from the grafting density. The bond orientation parameter exhibits some oscillations that mirror the layering observed in the segment density profiles and these oscillations become more pronounced at higher grafting densities (cf. Fig. 2). At very low grafting densities (i.e., in the mushroom regime) the bond orientation parameter rapidly decays for larger distances from the surface. At intermediate and large grafting densities, however, there is a pronounced perpendicular orientation of the bond vectors in the middle of the brush which stems from the stretching of the grafted chains. At the top of the brush the orientation parameter decays to zero.

Part (b) of Fig. 4 shows the corresponding orientation of free chains in the melt. In the ultimate vicinity of the grafting surface we find a pronounced parallel orientation similar to the first segments of the brush. Otherwise, the magnitude of the orientation of bond vectors in the melt is much smaller than for brush chains. There is only a small parallel alignment of the bond vectors that arises from the shear. It is slightly less pronounced inside the brush than in the middle of the film and there is a slight increase of alignment as we increase the grafting density. This can be rationalized as follows: The larger the grafting density, the higher is the velocity gradient in the middle of the film and the concomitant orientation (cf. the discussion of the slip length in subsection III D). The behavior is similar to the parallel alignment at a polymer-polymer interface or a substrate. It signals the formation of a well-defined brush-melt interface at high grafting densities and the difficulty of the free chains to penetrate into the brush which leads to autophobicity.

In panel (c) we investigate the behavior on larger length scales. Not surprisingly, orientation effects are much more developed for the radius of gyration than for bond vectors but the qualitative behavior is similar. Grafted chains with their centers of mass close to the grafting surface adopt pancake-like conformations that are more extended parallel to the wall than in the perpendicular direction. The majority of grafted chains have their mass centers in the middle of the brush region around $z \approx R_{ee}$ and they are extended away from the grafting surface. The effect increases for higher grafting densities and the further the chain's center of mass is displaced from the surface. Free chains in turn, are much less aligned and their parallel alignment arises from the shear, except for the two highest grafting densities, where one additionally observes a parallel alignment of chains at the brush-melt interface.

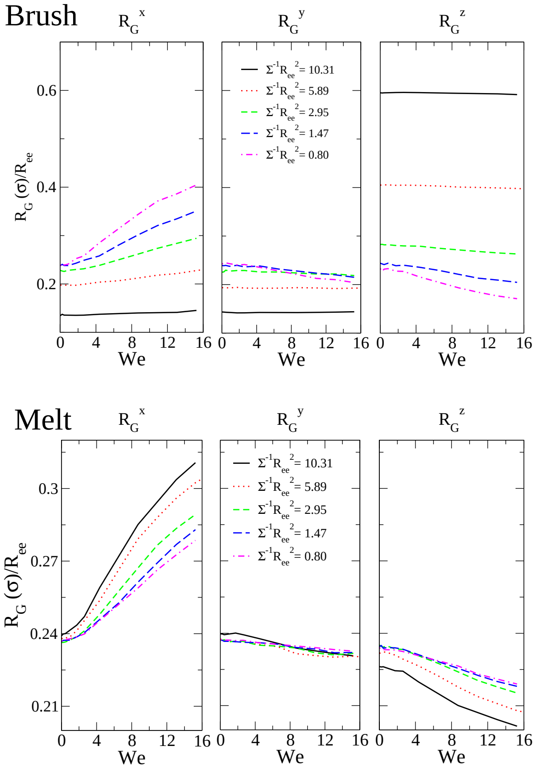

Figure 5: Cartesian components of the average radius of gyration as function of shear velocity, v_x, for grafted chains (top) and free chains of the melt (bottom). Different lines correspond to various grafting densities as indicated in the key. For a Gaussian chain each Cartesian component of the radius of gyration is given by $R_G^i = \frac{R_{ee}}{3\sqrt{2}}$.

In Fig. 5 we corroborate our findings by analyzing the behavior of the Cartesian components of the radius of gyration as a function of shear velocity. The data are averaged over all chains in the film independently of their distance from the surface. The top panel (a) shows the behavior of the brush. As we increase the grafting density the chains stretch away from the grafting surface. At high grafting density the chain conformation in the brush hardly depends on shear velocity. At lower grafting density, shear reduces the stretching perpendicular to the substrate but elongates the chains in the shear direction. The chain extension in the neutral direction, $\hat{y}$, is largely unaffected by shear but decreases as a function of grafting density. This effect is particularly pronounced for the rather short chains, $N = 10$, utilized in our simulations because the chain extension in the strongly stretched state is not very much smaller than the con-

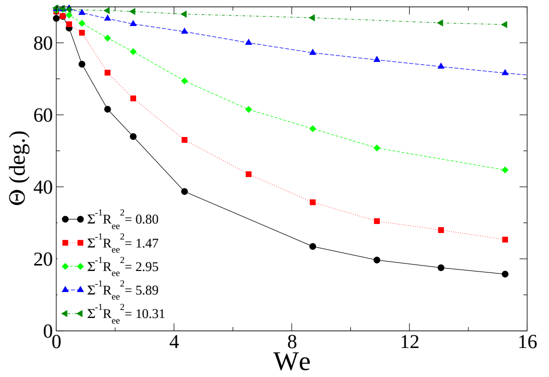

Figure 6: Average angle of the radius of gyration for the brush layer as a function of wall velocity for different grafting densities. $\Theta = 90$ corresponds to a brush completely perpendicular to the wall.

tour length and, thus, stretching reduces the fluctuations of the chain extension perpendicular to the stretching direction. For longer chains, however, we would expect a decoupling between the chain extension parallel and perpendicular to the substrate and, consequently, a smaller influence of the grafting density on R_G^y.

The behavior of the free chains is presented in panel (b). The dependence of the chain dimensions on the grafting density is rather weak. At vanishing shear velocity and high grafting density the chains are slightly aligned parallel to the brush-melt interface (x-y-plane). Fig. 4 suggest that similar orientation effects would also arise at the substrate for low grafting densities but there are very few melt chains in the film whose center of mass is in the vicinity of the grafting surface. Upon increasing the shear rate, we observe an orientation of the free chains in the shear direction.

It is of interest to study to what extend the conformational changes of brush and melt chains arise from orientation of the chains or from deformation of the chains. In Fig. 6 the average angle of the end-to-end vector of grafted chains with respect to the grafting surface is shown. This is defined as:

$$\Theta = 90^o - \arccos(\vec{R}_{ee} \cdot \hat{z}/R_{ee}),$$

where $\vec{R}_{ee}$ is the mean end-to-end vector and $\hat{z}$ is the direction perpendicular to the wall. Without shear, the average x and y coordinates of the brush segments coincide with the location of the grafting point in the x-y-plane and this configuration corresponds to an angle of 90^0. Upon shearing the film the chains tilt and the average angle decreases. The angle is smaller, the larger the shear rate and the lower the grafting density are chosen. For small shear rates the angle decreases roughly linear with the shear velocity, v_x, and saturation effects become apparent once the angle drops below 45^0.

In Fig. 7 (a), the orientation of the free chains in the middle of the film is shown for different length scales. The alignment with the shear direction is the more pronounced the larger the length scale and, analog to the behavior of the brush, the orientation effects depend roughly linearly on the shear rate.

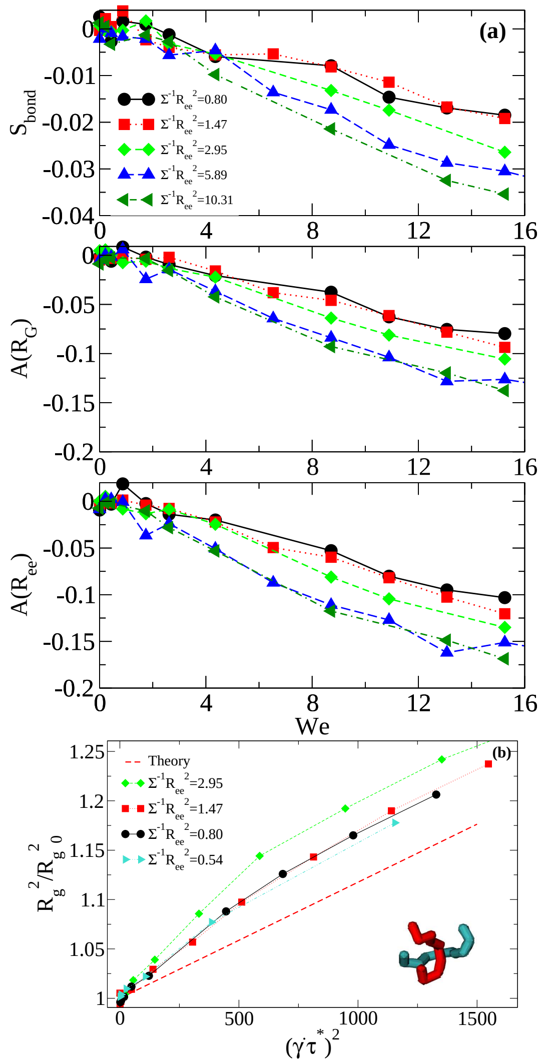

Figure 7: (a) Orientation of the free chains in the center of the film versus Weissenberg number. The different panels present the bond orientation parameter $S_{\rm bond}$ (top), the asphericity parameter for radius of gyration $\mathbf{R}_G$ (center), and end-to-end vector $\mathbf{R}_{ee}$ (bottom) for various grafting densities as indicated in the key, respectively. (b) Deformation of free chains in the center as a function of the adimensional shear rate. The theoretical results by Bruns[43] is indicated with dashed line. An example of the topological arrangement of the chains is shown in the inset.

This orientation effect contrasts with the deformation of the chain which can be measured by the change of the mean square radius of gyration. In Fig. 7 (b) we find that the coil deformation depends quadratically on the shear rate for small to intermediate shear velocities and a saturation appears for the highest shear rates. The data are averaged over the central region of the film considering a width of $1.4R_{ee}$. The shear rate is also evaluated there to assure a linear velocity profile, for a precise calculation of the shear rate. As showed in Fig. 7, the curves for different grafting densities collapse, except for the $\Sigma^{-1}R_{ee}^2 = 2.95$. This is expected due to the fact that, for this case, the melt density is not exactly $\rho\sigma^3 = 0.61$, as mentioned previously. The quadratic behavior finding is in accord with the theoretical prediction[43]:

$$R_G^2(\dot{\gamma}\tau) = R_G^2(0)(1 + \frac{(\dot{\gamma}\tau)^2}{8508}), \qquad (12)$$

where $R_G(0)$ is the radius of gyration at 0 shear rate. However, we see a difference with the slope predicted theoretically in the context of the Rouse model[44]. We attribute this to the topological interactions of the chains even though they are not long enough to be entangled (see an example taken from the simulation in the inset of 7(b)).

C. Viscosity of the melt

In Fig. 8 the velocity profiles of the melt under steady shear are presented. From the velocity profile of the melt in the center of the film we extract the shear viscosity, η, of the melt bulk phase according to

$$\eta = \frac{\langle F_x \rangle / A}{|\nabla v_x|}, \qquad (13)$$

where $\langle F_x \rangle$ denotes the mean force of the walls in the shear direction and A is the area of the substrate. ∇v is the velocity gradient at the center. We use the linear velocity profile in the middle of the film (cf. Fig. 8) to extract the gradient according to $|\nabla v_x| = \frac{v_x}{D_w/2+b}$, where D_w indicates the film thickness and b the slip length (see subsection III D).

The simulations were performed at constant volume and therefore the final value of the melt density in the middle of the film is unknown ahead of time and depends on how much the brush layer squeezes the melt. Consequently, we performed a first set of runs where the density in the melt slightly deviated from the target value, $\rho\sigma^3 = 0.61$, and then adjusted the number of chains in the simulation cell. Alternatively, we could have simulated at constant normal pressure. The results of the simulations with constant density in the middle of the film are shown in figure Fig. 9 for the grafting densities $R_{ee}^2/\Sigma = 2.95$, 5.89 and 10.31. We observe *shear thinning* typical of non-Newtonian fluids in the studied range of velocities which becomes very pronounced at even higher shear rates. In the regime of very low shear rates, the data have rather large error bars because of the very high fluctuations of force in the shear direction. The error bars shown in the figure are obtained from a block average analysis[40] of the wall force, F_x. This low signal-to-noise ratio makes it difficult an extrapolation to the viscosity at vanishing shear rate.

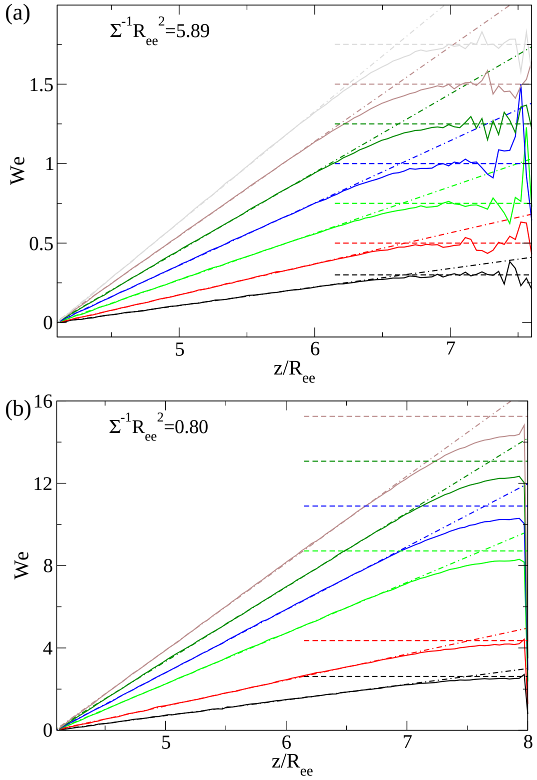

Figure 8: Velocity profiles as function of wall velocity for: (a) grafting density $R_{ee}^2/\Sigma = 5.89$ and (b) $R_{ee}^2/\Sigma = 0.80$. The wall (and brush layer) velocity is indicated with dashed horizontal lines. Dashed-dotted lines show the linear extrapolation of the far-field velocity. In the first case stick boundary condition is observed for the fluid in the melt-brush interface. The latter case corresponds to a finite slip boundary condition in which the fluid never reaches the brush layer velocity.

A more reliable estimate of the viscosity at zero shear rate can be obtained from the Green-Kubo formula.[45] To this end we performed simulations of the bulk system with periodic boundary conditions in three dimensions at density $\rho_{\mathrm{melt,coex}}\sigma^3 = 0.61$. The viscosity can be calculated from equilibrium simulations as the time integral of the pressure tensor correlation function:[45]

$$\eta_{\mathrm{GK}}(t) = \frac{V}{k_B T} \int_0^t \mathrm{d}t' \, \left\langle P^{\alpha\beta}(t') \cdot P^{\alpha\beta}(0) \right\rangle, \qquad (14)$$

where V is the volume of the system and the pressure tensor $P^{\alpha\beta}$ is given by:

$$P^{\alpha\beta} = \frac{1}{V} \left(\sum_i m v_i^\alpha v_i^\beta + \sum_{i<j} F_{ij}^\alpha r_{ij}^\beta \right) \quad . \qquad (15)$$

Since the pressure tensor is a collective quantity 10 independent simulation runs with 4×10^6 steps each ($dt = 0.002\tau$) were needed for an accurate result. The average,

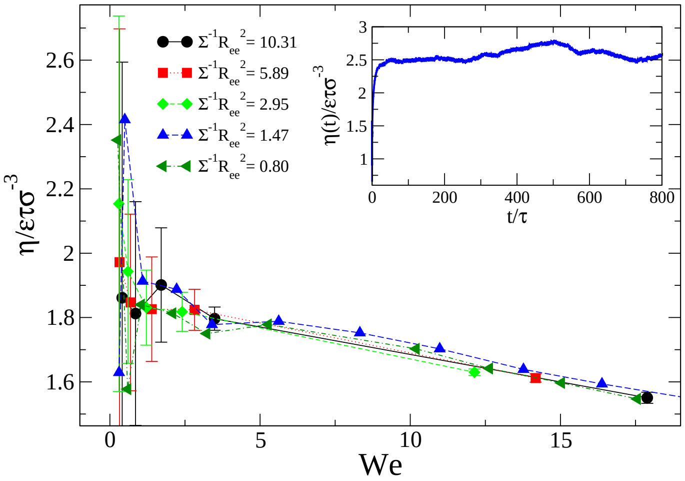

Figure 9: Viscosity of the melt as a function of the shear velocity for the studied grafting densities. The melt density, indicated in the legends was set to $\rho = 0.61\sigma^{-3}$. The inset shows the viscosity as a function of t as given by the Green Kubo formula.

$\eta_{\rm GK}(t)$ in Eq. (14), over the 10 independent runs is displayed in the inset of Fig. 9. Our final estimate for the bulk viscosity is $\eta_{\rm GK} = 2.5(3)$. Within the error bars this value is compatible with the extrapolation of the zero-shear-rate viscosity from the non-equilibrium simulation. It seems that the estimates of the non-equilibrium simulations are systematically lower than the results from the bulk fluctuation analysis. If there really is a systematic discrepancy, it might be attributed to the rather small film thickness in the shear simulations. Especially at high grafting densities, where the deviations are the largest, the "bulk-like" middle of the film is rather narrow and the brush-melt interface tends to align the chains in the direction of the shear resulting in a somewhat lower estimate for η.

D. Effective boundary condition and slip length

In order to exploit polymer brushes as soft, deformable surface coatings in micro- and nanofluidic devices two key characteristics of the brush have to be controlled: (i) the wetting properties of the liquid on top of the brush and (ii) the boundary condition which describes the velocity field of the fluid in the vicinity of the surface. Typically, one encodes the microscopic structure and dynamics at the surface in a single parameter, the slip length b, which is defined as the distance, $z = -b$, behind the substrate where the extrapolation of the linear, far-field velocity profile, $v(z)$, attains the substrate velocity, v_x, as assumed by a macroscopic no-slip boundary condition. A positive value of the slip length, b, implies that the fluid velocity at the solid surface does not reach the substrate velocity, i.e., there is slip at the grafting surface, and the extrapolated velocity profile reaches the surface velocity, v_x, inside the solid substrate.

The velocity profiles in Fig. 8 also provide information about the hydrodynamic boundary condition. The velocity of the brush segments coincides with the velocity of the wall, v_x, of course, and it is indicated by horizontal lines. For the free chains of the melt we observe two different behaviors as a function of grafting density:

For medium to higher grafting densities (R_{ee}^2/Σ = 2.95, 5.89, 10.31) the liquid flow on top of the brush is described by a *stick* boundary condition, in which the melt reaches the wall (brush) velocity for all shear rates studied.[46] For instance, in Fig. 8(a) the velocity profile of a liquid over a densely grafted brush, $R_{ee}^2/\Sigma = 5.89$, is shown for different shear rates. As one can observe, the boundary velocity is, in fact, attained before the substrate and free chains that are inside the brush are completely entrained. This corresponds to a negative slip length and characterizes the hydrodynamic thickness of the brush.[22]

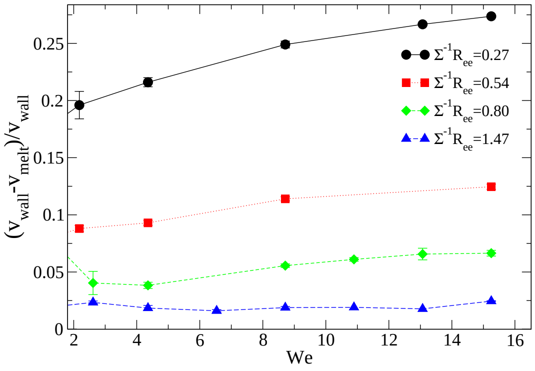

Figure 10: Relative slip velocity of the melt as a function of shear velocity for those grafting densities that have partial slip boundary conditions.

At lower grafting densities (R_{ee}^2/Σ = 0.27, 0.54, 0.80, 1.47), however, the boundary condition of the melt changes toward a *finite slip*. The melt never reaches the velocity of the grafting substrate, and the slip at the substrate increases as we decrease the grafting density. In Fig. 10 the slip velocity of the melt at the substrate is shown as a function of shear velocity for the smallest grafting densities. The boundary condition for these grafting densities that results in partial slip was also studied as a function of time. Often experiments report stick-slip boundary condition[27], where the fluid motion switches from complete stick to complete slip in the course of time. We did not observe this phenomenon in the time window considered in the simulations. The system rather exhibits a steady partial slip as observed from the time dependence of the shear force.

Figure 8(b) displays the velocity profile for various shear velocities. Although there is a notable microscopic slip at the substrate the concomitant slip length, b, extrapolated from the far-field velocity profile is very small and negative because the velocity profile strongly deviates from the linear behavior assumed in the extrapolation of the far-field velocity. Thus, microscopic slip velocity and distortion of the velocity profile at the substrate compensate each other and the *effective* boundary condition corresponds to no slip.

In the limit of extremely low grafting densities ($R_{ee}^2/\Sigma = 0.27$), we observed a positive slip length (see inset of Fig. 12): Although the liquid wets the solid substrate, in the limit of no grafted chains, $R_{ee}^2/\Sigma = 0$, there is complete slip at the substrate (i.e., $b \to \infty$) because it is perfectly flat.

We performed simulations of a single chain grafted to the wall to analyze the influence and spacial extension of the perturbation in the melt fluid velocity. The capacity of a single chain to drag is isolated in this way. The comparisson of the mean fluid velocity in the shear direction is presented in Fig. 11 for a wall velocity of We=8.71. The system of coordinates was taken to be in the wall, therefore a smaller velocity means that the grafted chain is dragging the fluid along. Far from the grafted chain a high velocity is observed. Panel (a) shows the density of beads belonging to the grafting chain and the decay of the fluid velocity along and also perpendicular to the shear direction. The asymmetry, with enhancement in the shear direction is due to the deformation of the grafted chain in this direction, as can be clearly observed in Fig. 11(b) for a plane close to the grafting point.

The mean slip length, b, as a function of grafting density and Weissenberg number is plotted in Fig. 12. b is rather insensitive to the shear rate, except for the lowest grafting density considered, $R_{ee}^2/\Sigma = 0.27$, that shows a clear dependence with the shear rate. At very high grafting densities, the slip length is negative and its absolute magnitude is comparable but slightly smaller than the thickness of the dense brush (cf. Fig. 2). At high grafting densities the slip length does not strongly depend on the shear rate in accord with the insensitivity of the density profiles in this regime.

The errors in the slip length in Fig. 12 increase significantly for small grafting densities. Note that the chains are grafted randomly and for low grafting densities (mushroom regime), when the grafted chains do not strongly overlap, the influence of the grafted chains in the fluid is not homogeneous and quenched fluctuations of the grafting points become important (a limiting case is showed in Fig. 11 for a single grafted chain). This gives rise to sample-to-sample fluctuations which can be observed via the slight asymmetry of the velocity profile across the simulation cell. Therefore the error is large at low grafting densities at low grafting densities.

As we reduce the grafting density the slip length increases. In this regime, b characterizes the rather intricate interplay between different factors: (i) As the grafting density decreases the physical thickness of the brush decreases leading to less negative values of b. (ii) Additionally, the melt chains penetrate deeper into the brush (cf. Fig. 3) resulting in a hydrodynamic thickness that is smaller than the physical thickness.[22] (iii) At low enough grafting densities there is microscopic slip corresponding to an incomplete entrainment of the melt by the brush. Eventually, the slip length will diverge as the grafting density vanishes because of our choice of a perfectly smooth substrate that exhibits complete slip.

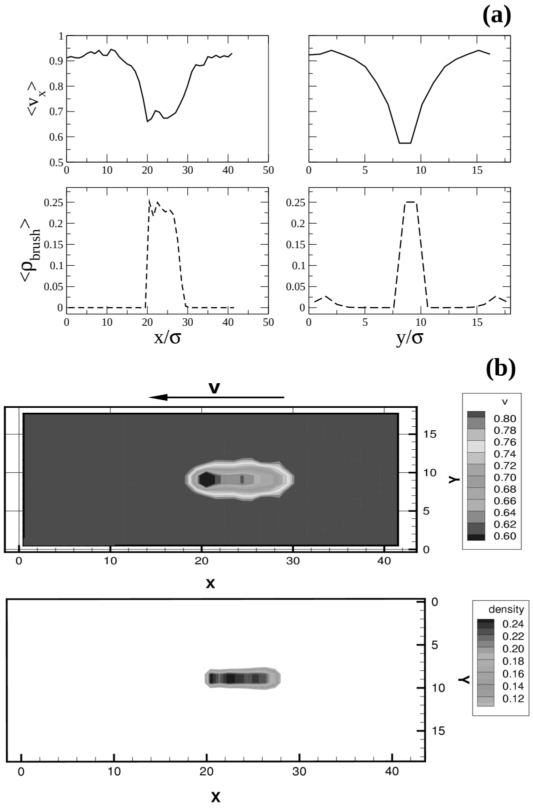

Figure 11: (a) Average melt velocity in the shear direction (plain line) and density of beads belonging to a grafted chain (dashed line). The left panel shows the profile along the shear direction and the right one in the perpendicular one. This simulation was performed with one chain grafted in the surface. Panel (b) shows the two dimensional profile of melt velocity (up) and bead density (down) in a plane close to the grafting position $z \sim 1.2\sigma$. The center correspond to the position in which the chain is grafted. The shape and extension of the influence of the grafted chain in the melt velocities can be clearly observed.

These results suggest that the boundary condition of the liquid flow on top of the brush can be controlled by changing only the grafting density, which is readily accessible in experiments. This offers opportunities for studying flows whose boundary conditions are purely entropically tunable without any change in the chemical nature of the macromolecules or the substrate.

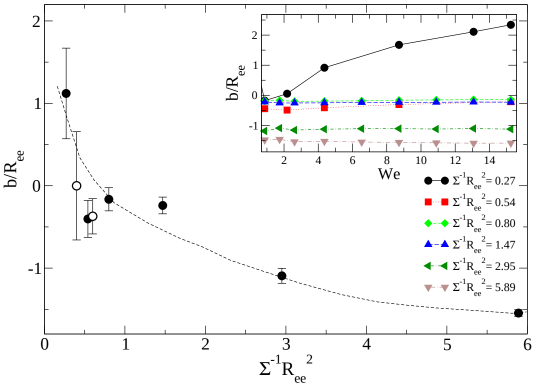

Figure 12: Slip length as a function of grafting density for various grafting densities, that give rise to stick and partial slip boundary conditions. The points indicated with open circles correspond to runs made only for We= 8.71 and the dashed line is a guide for the eyes. The slip length b versus Weissenberg number is presented in the inset.

IV. CONCLUSIONS

In this work, the interface between a brush and a melt was investigated in equilibrium and under shear as a function of the sliding velocities of the walls and for a wide range of grafting densities of the brush layer. The polymers of both, brush and melt, were taken to be physically identical and described by a coarse-grained bead-spring model. Polymer segments attracted each other corresponding to a bad solvent below the Θ-temperature. We used the DPD thermostat to duly account for the hydrodynamic interactions in the system.

The building-up of the brush-melt interface was observed and characterized upon increasing grafting densities: As expected, free melt chains were progressively expelled from the polymer brush layer as we increase the grafting density. The melt chains orient parallel to the brush-melt interface and bond vectors align much less than the end-to-end vector. This behavior is similar to what is observed at interfaces between immiscible polymers but here it occurs at an interface between chemically identical species and is solely due to entropic effects. The pronounced structural changes at the brush-melt interface also suggest that there is a free energy cost associated with this interface which will lead to autophobicity, i.e. the dewetting of the melt of identical chains from the brush. This was confirmed by setting up a droplet on the top of the brush layer which proved to be stable exactly for the same thermodynamic parameters than those used in the shear simulations. The behavior of droplets on this autophobic substrate will be the subject of a future publication.

We complement the equilibrium information with the response of the brush-melt interface to shear. From the gradient of the velocity at the center of the film and via correlations of the pressure tensor in equilibrium we have estimated the shear viscosity of the bulk phase. The density profiles also provide information about the hydrodynamic boundary condition. For low grafting densities a partial-slip boundary condition was found and the interface structure is strongly affected by shear. At larger grafting densities, however, the simulation data are well describable by a stick boundary condition and the brush is only very little affected by shear[46]. Stick-slip phenomena could not be detected during the time window of our simulation. Thus, a dense brush is efficient in dragging along the polymer melt even though thermodynamically it would dewet (at coexistence pressure). This is a first step towards describing the motion of droplets on this soft, deformable brush substrate. One key result of our study is the ability to change the thermodynamic properties and hydrodynamic boundary conditions of a melt in contact with a substrate by changing only the grafting density which is an experimentally accessible parameter. We note that the cross-over towards autophobic behavior and from slip to stick boundary conditions occurs when the chains of the brush begin to overlap, i.e. at rather moderate grafting densities.

Acknowledgments

It is pleasure to thank Luis Gonzalez MacDowell, Jörg Baschnagel and Joachim Wittmer for useful discussions. Financial support by the DFG within the priority program “Micro- und Nanofluidik” Mu 1674/3-1 and the ESF-program STIPOMAT are gratefully acknowledged. Computing time was provided by the NIC, Jülich, Germany.

---

[1] *Polymer Brushes*, R.C. Advincula, W.J. Brittain, K.V. Caster, and J. Rühe, , (Eds.) WILEY-VCH, Weinheim (2004).

[2] J. Klein, Kumacheva E., D. Mahalu, D. Perahia, and L. J. Fetters, Nature **370**, 634 (1994).

[3] S.T. Milner, T.A. Witten, and M.E. Cates, Macromolecules **21**, 2160 (1988).

[4] L. Leibler, A. Adjari, A. Mourran, G. Coulon, and D. Chatenay, in *OUMS Conference on Ordering in Macromolecular systems*, Osaka, Springer-Verlag, Berlin (1994); P.G. Ferreira, A. Ajdari, and L. Leibler, Macromolecules **31**, 3994 (1998).

[5] M.W. Matsen and J.M. Gardiner, J. Chem. Phys. **115**, 2794 (2001); M.W. Matsen, J. Chem. Phys. **117**, 2351 (2002).

[6] J.H. Maas, G.J. Fleer, F.A.M. Leermakers, and M.A. Cohen-Stuart, Langmuir **18**, 8871 (2002); F.A.M. Leermakers, J.H. Maas, and M.A. Cohen-Stuart, Phys. Rev. **E**

66, 051801 (2002).

[7] Müller, M. and MacDowell, LG, Europhys. Lett. **55**, 221 (2001).

[8] L.G. MacDowell and M. Müller, preprint, submitted to J.Phys.: Condens. Matter (2005)

[9] T. Kerle, R. Yerushalmi-Rosen, and J. Klein, Europhys. Lett. **38**, 207 (1997); Macromolecules **31**, 422 (1998); J. Jopp and R. Yerushalmi-Rosen, Macromolecules **32**, 7269 (1999).

[10] G. Reiter and R. Khanna, Phys. Rev. Lett. **85**, 5599 (2000).

[11] A. Voronov and O. Shafranska, Langmuir **18**, 4471 (2002); Polymer **44**, 277 (2003).

[12] L. Leibler, Makromol. Chem. Macromol. Symp. **16**, 1 (1988).

[13] K.S. Shull, E.J. Kramer, G. Hadziioannou, and W. Tang. Macromolecules **23**, 4780 (1990).

[14] H.R. Brown, Macromolecules **22**, 2859 (1989); H.R. Brown, V.R. Deline, P.F. Green, Nature 1989, **341**, 221 (1989); H.R. Brown, K. Char, V.R. Deline, P.F. Green, Macromolecules **26**, 4155 (1993).

[15] S.T. Milner, MRS Bull. **22**, 38 (1997).

[16] M.E.R. Shanahan, J. Phys. **D 12**, 1473 (1979); A. Carre and M.E.R. Shanahan, Langmuir **17**, 2982 (2001).

[17] G. Reiter, J. Schultz, P. Auroy, and L. Auvray, Europhys. Lett. **33**, 29 (1996).

[18] P. Lai and K. Binder, J. Chem. Phys. **95**, 9288 (1991).

[19] P. Lai and K. Binder, J. Chem. Phys. **97**, 586 (1992).

[20] G. S. Grest, M. Murat , *Monte Carlo and Molecular Dynamics Simulations in Polymer Science*, K. Binder (Ed.) , Oxford Univ. Press, New York (1995).

[21] G.S. Grest, J. Chem. Phys. **105**, 5532 (1996).

[22] P.S. Doyle, E.S.G. Shaqfeh, and A.P. Gast, Macromolecules **31**, 5474 (1998).

[23] K.Ch. Daoulas, A.F. Terzis, and V.G. Mavrantzas, J. Chem. Phys. **116**, 11028 (2002).

[24] S. W. Sides, G. S. Grest , and M. J. Stevens, Phys. Rev. E **64**, 050802 (2001).

[25] C. Cottin-Bizonne, J. L. Barrat , L. Bocquet, and E. Charlaix, Nature Materials **2**, 237 (2003).

[26] K. M. Awati, Y. Park, E. Weisser, and M. E. Mackay, J. Non-Newtonian Fluid Mech. **89**, 117 (2000).

[27] L. Bureau and L. Léger, Langmuir **20**, 4523 (2004).

[28] F. Varnik and K. Binder , J. Chem. Phys. **117**, 6336 (2001).

[29] N. V. Priezjev and S. M. Troian , Phys. Rev. Lett. **92**, 18302 (2004).

[30] F. Brochard-Wyart, C. Gay , and P. G. de Gennes, Macromolecules **29**, 377 (1996).

[31] L. Bocquet and J.-L. Barrat, Phys. Rev. **E 49**, 3079 (1994); Phys. Rev. Lett. **82**, 4671 (1999).

[32] T. Kreer, M. Müser, K. Binder, and J. Klein, Langmuir **17**, 7804 (2001).

[33] T. Kreer, K. Binder, and M. Müser, Langmuir **19**, 7551 (2003).

[34] G. S. Grest and K. Kremer, Phys. Rev A **33**, 3628 (1990).

[35] M. Kröger, Phys. Rep. **390**, 453 (2004).

[36] T. Kreer, S. Metzger, M. Müller, K. Binder, and J. Baschnagel, J. Chem. Phys. **120**, 4012 (2004).

[37] Müller, M. and MacDowell, LG, Macromolecules **33**, 3902 (2000).

[38] P. J. Hoogerbrugge and J. M. V. A. Koelman, Europhys. Lett. **19**, 155 (1992).

[39] P. Español and P. Warren, Europhys. Lett. **30**, 191 (1995).

[40] B. Smit and D. Frenkel, *Understanding Molecular Simulation, Second Edition* (Academic Press, 2002).

[41] M. P. Allen and D. J. Tildesley, *Computer simulation of liquids* (Clarendon Press, Oxford, 1990).

[42] T. Soddemann, B, Dünweg, and K. Kremer, Phys. Rev. E **68**, 46702 (2003).

[43] W. Bruns and W. Carl, Macromolecules **26**, 557 (1993).

[44] M. Doi and S. F. Edwards, *The Theory of Polymer Dynamics, Second Edition* (Clarendon Press, Oxford, 1986).

[45] J. P. Hansen and I. R. McDonald, *Theory of Simple Liquids* (Academic Press, 1986).

[46] At extremely high grafting densities we expect the interdigitation between brush and melt to become so small (c.f. Fig. 3a) that the finite slip might occur.